NOX2 inhibition enables retention of the circadian clock in BV2 microglia and primary macrophages

Iswarya Muthukumarasamy[1,2], Sharleen M. Buel[2,3], Jennifer M. Hurley[2,3] and Jonathan S. Dordick[1,2,3]*

[1]Chemical and Biological Engineering, Rensselaer Polytechnic Institute, Troy, NY, United States, [2]Center for Biotechnology & Interdisciplinary Studies, Rensselaer Polytechnic Institute, Troy, NY, United States, [3]Biological Sciences, Rensselaer Polytechnic Institute, Troy, NY, United States

Introduction: Sustained neuroinflammation is a major contributor to the progression of neurodegenerative diseases such as Alzheimer's (AD) and Parkinson's (PD) diseases. Neuroinflammation, like other cellular processes, is affected by the circadian clock. Microglia, the resident immune cells in the brain, act as major contributors to neuroinflammation and are under the influence of the circadian clock. Microglial responses such as activation, recruitment, and cytokine expression are rhythmic in their response to various stimuli. While the link between circadian rhythms and neuroinflammation is clear, significant gaps remain in our understanding of this complex relationship. To gain a greater understanding of this relationship, the interaction between the microglial circadian clock and the enzyme NADPH Oxidase Isoform 2 (NOX2) was studied; NOX2 is essential for the production of reactive oxygen species (ROS) in oxidative stress, an integral characteristic of neuroinflammation.

Methods: BV2 microglia were examined over circadian time, demonstrating oscillations of the clock genes *Per2* and *Bmal1* and the NOX2 subunits gp91phox and p47phox.

Results: The BV2 microglial clock exerted significant control over NOX2 expression and inhibition of NOX2 enabled the microglia to retain a functional circadian clock while reducing levels of ROS and inflammatory cytokines. These trends were mirrored in mouse bone marrow-derived primary macrophages.

Conclusions: NOX2 plays a crucial role in the interaction between the circadian clock and the activation of microglia/macrophages into their pro-inflammatory state, which has important implications in the control of neuroinflammation.

Abbreviations: AD, Alzheimer's Disease; PD, Parkinson's Disease; Apo, Apocynin; BMDMs, Bone Marrow Derived Macrophages; CT, Circadian Time; DPI, Diphenyleneiodonium chloride; GSK, GSK2795039; HPS, Hours Post Serum Shock; IFN-γ, Interferon Gamma; TNF-α, Tumor Necrosis Factor Alpha; IL-6, Interleukin 6; IL-4, Interleukin 4; NADPH, Nicotinamide Adenine Dinucleotide Phosphate; NOX2, NADPH Oxidase Isoform 2; ROS, Reactive Oxygen Species; TTFL, Transcriptional-Translational Feedback Loop.

Introduction

Microglia, the innate immune cells of the central nervous system, are involved in inflammation and the immune response, and play a significant role in contributing to neuroinflammation associated with neurodegenerative diseases (1). Like macrophages, microglia display multiple phenotypes based on external stimuli, and are normally distinguished into resting and activated states in the brain (2). In their resting state, microglia carry out continuous surveillance of the central nervous system to maintain homeostasis (2). The activated microglial state is itself an oversimplification and comprises multiple phenotypes (3, 4), broadly differentiated into pro-inflammatory and anti-inflammatory states (3, 4). The pro-inflammatory phenotype is associated with the release of mediators that lead to inflammation (5–7), whereas the anti-inflammatory phenotype is associated with the release of mediators that promote wound healing and debris clearance (4, 8, 9). Under normal healthy conditions, there is a fine balance between these phenotypes, which ensures homeostasis. However, in the case of various neurodegenerative diseases, the intricate balance among microglial phenotypes is lost and there is sustained activation of microglia into a pro-inflammatory state, resulting in neuroinflammation (4, 10). Such chronic neuroinflammation has been associated with the progression of various neurodegenerative diseases such as Alzheimer's (AD) and Parkinson's (PD) diseases, among others, making neuroinflammation a potential target for therapeutic intervention.

A predominant aspect of the microglial pro-inflammatory response is the release of reactive oxygen species (ROS), which is facilitated by the enzyme NADPH oxidase isoform 2 (NOX2) (11). ROS generated by NOX2 is normally under tight control of various protective enzymes, including catalases, superoxide dismutases, and glutathione peroxidases, as well as small molecule antioxidants (12). When such regulatory processes fail, the cell enters a state of oxidative stress (13). The overproduction of ROS combined with the reduced activity of ROS scavenging enzymes results in oxidative damage of biomolecules and neurons (12, 14, 15), making NOX2 an attractive target to combat chronic neuroinflammation (16, 17).

The immune responses, including neuroinflammatory responses, are tightly controlled by the circadian clock (18). Circadian clocks are broadly present in organisms that live in the photic zone and ensure efficient synchronization between physiologic functions and the 24 h structure of the day (19). This time-based regulation by the circadian clock is facilitated through a transcriptional-translational negative feedback loop (TTFL) orchestrated by a pair of transcriptional activators/repressors (20). Through this intricate feedback loop, the circadian clock ensures the oscillation of a broad array of genes and proteins to time cellular physiology. At the cellular level, macrophages and monocytes have robust circadian clocks with high amplitude oscillations of their core clock genes and proteins (21, 22). This strong influence of the circadian clock over immune cell physiology results in 24 h rhythms in levels of cytokines, recruitment of macrophages and monocytes to tissues, phagocytosis, and response of pattern recognition receptors (18). Paralleling what is observed in macrophages, microglia also display high amplitude rhythms in circadian clock genes and inflammatory cytokines (23, 24).

Disruption of the circadian clock has been associated with increased risk for, and progression of, disease states, particularly diseases with inflammatory components (19, 25–28), including neurodegenerative diseases (28, 29). Mouse models have shown that impairment of the microglial clock results in increased levels of inflammation and worsening of AD symptoms (30). In parallel, activation of macrophages into pro- and anti-inflammatory phenotypes directly modulates the function of the circadian clock (31), indicating the complex relationship between inflammatory responses, the circadian clock, and disease states. Although the fields of circadian biology and neuroinflammation have advanced exponentially in recent years, there remain significant gaps in our understanding of the interrelationship between circadian rhythms and neuroinflammation. Gaining a mechanistic insight into this intricate relationship may advance the development of interventional therapies that mitigate circadian disruption thereby preventing neuroinflammation associated with various neurodegenerative diseases.

The strong dependence of neuroinflammation on NOX2 activation (14, 32–34) and circadian disruption (18, 21, 35, 36) has been studied individually, but the correlation between NOX2 activation and circadian disruption has yet to be explored in depth. In the current study, the influence of the circadian clock in a BV2 microglial cell line has been investigated, specifically with respect to NOX2 expression. Activation of BV2 microglia into pro- or anti-inflammatory phenotypes resulted in distinct effects similar to those observed in macrophages, with the clock losing its rhythm under pro-inflammatory activation and retaining its rhythm under anti-inflammatory activation (31). Furthermore, the circadian clock in BV2 microglia exerted strong control over the expression of various NOX2 enzyme subunits. Inhibition of NOX2 in a pro-inflammatory state resulted in retention of a functional circadian clock, suggesting that NOX2 plays an important role in the connection between neuroinflammation and circadian disruption in the context of neurodegenerative diseases. Finally, we found the link between the clock and NOX2 in BV2 cells consistent with data from primary bone marrow-derived mouse macrophages, indicating a conserved connection between NOX2 and the clock in cells involved in the inflammatory response.

Materials and methods

Materials

The BV2 mouse microglial cell line was obtained from Banca Cellule ICLC, Genova, Italy. Lipopolysaccharide (LPS) 500X was obtained from Invitrogen (Waltham, MA). Murine IL-4 was obtained from Peprotech Inc. (Rocky Hill, NJ). NOX2 inhibitors apocynin and GSK2795039 (GSK) were purchased from Millipore Sigma (Burlington, MA) and MedChemExpress (Monmouth Junction, NJ), respectively. Primary antibodies against phospho-p47^{phox} (Ser 370), PER2, and BMAL1, and goat anti-rabbit secondary antibody were obtained from Invitrogen. Phosphate buffered saline (PBS) and trypsin-EDTA for cell culture were

BV2 cell culture and synchronization

BV2 cells were cultured in RPMI-1640 medium (ThermoFisher Scientific) with L-glutamine (2 mM) and supplemented with 10% heat-inactivated FBS (ThermoFisher Scientific). All circadian studies used a serum-shock method to synchronize the cells (22). The cells were plated in normal growth media (RPMI + 10% FBS) at a density of 10^5 cells/mL in 6-well plates and allowed to reach 90% confluence. Culture media was then replaced with starvation media (RPMI) for 24 h. Following media starvation, the cells were subjected to serum-shock using 50% FBS for 2 h to synchronize their clock (22, 37–39). Post-serum shock, normal growth media was used, and the cells were allowed to recover for 16 h from the serum-shock and attain homeostasis. Samples were collected every 2 h for 24 h, starting at 16 h post serum-shock (Hours Post Serum Shock 16 or HPS16), and processed for RT-qPCR and Western blotting.

Bone marrow derived macrophage extraction and synchronization

Bone marrow was extracted from the tibias and femurs of 3-6 month old male *Per2:Luc* (C57BL/6J) mice. The bone marrow progenitor cells plated on 35 mm cell culture plates, were differentiated with DMEM supplemented with M-CSF and 10%FBS as mentioned in a previous protocol (22, 39). After 7 days, the differentiated macrophages were synchronized by a 24 h starve in serum-free media followed by a 2 h serum-shock with 50% FBS as mentioned previously (22, 39). Post serum-shock synchronization, cultures were sealed with grease and glass cover slips and luminescence was measured over a period of 5 days using LumiCycle32 (Actimetrics, Wilmette, IL) with cells plated in Leibovitz media containing Luciferin and 10% FBS (22, 39).

Quantitative real-time PCR

The High Pure RNA Isolation Kit from Roche Molecular Systems, Inc. (Branchburg, NJ) was used for RNA extraction and purification. Purified RNA was reverse-transcribed using the High-Capacity cDNA Reverse Transcription Kit (ThermoFisher Scientific). mRNA abundance was determined by quantitative PCR using TaqMan Gene Expression Master Mix (Applied Biosystems, Waltham, MA) and the following pre-designed TaqMan primer assays: *Per2* (Assay ID: Mm00478099_m1), *Bmal1* (Assay ID: Mm00500223_m1), *Hprt1* (Assay ID: Mm03024075_m1), $p47^{phox}$ (Assay ID: Mm00447921_m1) and $gp91^{phox}$ (Assay ID: Mm01287743_m1). *Hprt1* was used as the reference gene for all RT-qPCR experiments. Data obtained from RT-qPCR was then input into the ECHO software (see Supplementary Information) for analysis of oscillation of gene expression (40).

Western blotting

Western blotting was used to investigate the oscillation of PER2 and BMAL1 clock proteins, and for quantification of phosphorylated-$p47^{phox}$ levels in BV2 microglia. Time course samples were collected from synchronized BV2 cells as described above. For measurement of phospho-$p47^{phox}$ levels, BV2 cells were plated in 6-well plates at a density of 10^5 cells/mL and allowed to reach 90% confluence. At confluence, cells were treated with LPS (1 μg/mL), or LPS (1 μg/mL) + apocynin (100 μM), or LPS (1 μg/mL) + GSK2795039 (25 μM) for 24 h. BV2 cells with no additives were used as a control. For all samples, cells were washed with ice-cold PBS and lysed with RIPA lysis buffer (Millipore Sigma, Burlington, MA) containing the Halt Protease Inhibitor Cocktail (ThermoFischer Scientific). Protein concentrations were measured using the Pierce BCA Protein Assay Kit (Pierce, Waltham, MA). Samples were loaded at 25 μg of total protein per lane, resolved by SDS-PAGE (BioRad, Hercules, CA), and transferred onto nitrocellulose membranes (Bio-Rad). Following blocking with 5% skim milk in PBST (137 mM NaCl, 2.7 mM KCl, 10 mM Na_2HPO_4, 1.8 mM KH_2PO_4, pH 7.4, 0.2% Tween-20) for 2 h at room temperature, the membranes were incubated with primary antibodies against PER2 (1:1000, Invitrogen, Waltham, MA), BMAL1 (1:1000, Invitrogen), and phospho-$p47^{phox}$ (Ser 370) (1:1000, Invitrogen) at 4^0C in 1% skim milk in PBST overnight. Post-overnight incubation, the membranes were washed six times with PBST and incubated with secondary antibody (1:10,000) for 1 h. The membranes were then washed with PBST, and the protein bands were detected using SuperSignal West Pico Chemiluminescent Substrate (Pierce). Amido black staining (see below) was used to normalize protein loading. Protein bands were detected using the BioRad ChemiDoc XRS+ Imager (BioRad). Quantification of detected protein bands was performed with the ImageLab 6.0.1 software (Life Science, Waltham, MA).

Amido Black staining

Amido Black staining was used to measure total protein loaded in a lane as the internal loading-control for Western blots. Following detection of protein bands, membranes were washed three times in DI water. The membranes were then stained for 1 min using a staining solution containing 0.1% amido black reagent in 10% acetic acid solution. The membranes were then washed twice for 1 min with a de-staining solution containing 5% acetic acid. Post de-staining, the membranes were washed two times for 10 min each in DI water. The membranes were then air-dried and visualized using a Bio-Rad ChemiDoc XRS+ Imager. Quantification of amido black stained membranes was done using the ImageLab 6.0.1 software.

ECHO analysis

ECHO version 4.1 was used to analyze all transcriptional and protein data obtained from the time-course experiments (40). All data was free run with the 'smooth data' and 'linear detrend' options selected. For transcriptional data, the 'normalize data' option was also selected. Data obtained from ECHO analysis was then transferred and

re-plotted on GraphPad Prism 7 (GraphPad Software, CA, USA). Details about the ECHO software and ECHO data for all transcriptome and proteome oscillations are available in the Additional File 6: Table S1.

ROS determination

ROS released by BV2 in the presence of LPS (1 µg/mL) and NOX2 inhibitors apocynin (100 µM) and GSK2795039 (25 µM) was measured using two different assays. The DCFDA/H2DCFDA Cellular ROS Assay Kit (Abcam, MA) was used to measure the levels of intracellular superoxide produced and the Amplex Red Hydrogen Peroxide/Peroxidase Assay kit (Invitrogen) was used to measure the levels of extracellular hydrogen peroxide produced in BV2 cells. Cells were plated in 96-well black-walled flat-bottom plates at a density of 10^5 cells/mL. The cells were incubated with LPS with and without a NOX2 inhibitor for 2 h in the assay media and fluorescence was measured using a SpectraMax plate reader (Molecular Devices, San Jose, CA). Fluorescence values were normalized to cell number measured using the Presto Blue Cell Viability Assay (ThermoFischer Scientific) as described below.

Cell viability determination

BV2 cells were seeded in 96-well flat-bottom, black-walled plates at a density of 10^4 cells/well and allowed to reach 90% confluence. The cells were then treated with media containing different additives. The media was then removed from each well and replaced with 90 µL fresh media and 10 µL PrestoBlue reagent (ThermoFisher Scientific) and incubated at 37°C and 5% CO_2 for 10 min. Fluorescence was measured at Ex/Em = 560/590 nm and cell numbers were correlated against a standard curve.

ELISA

A sandwich enzyme-linked immunosorbent assay (ELISA) was used to quantify cytokines produced by BV2 cells and primary macrophages. The cells were plated in 96-well plates at a density of 10^5 cells/mL and allowed to reach 90% confluence. The cells were then incubated for 24 h with media containing the following combination of additives: LPS (1 µg/mL); LPS (1 µg/mL) + apocynin (100 µM); apocynin (100 µM); LPS (1 µg/mL) + GSK (25 µM); and GSK (25 µM). To understand the influence of IL-4 addition on cytokine production, cells were incubated with the following combination of additives: IL-4 (20 ng/mL); LPS (1 µg/mL); IL-4 (20 ng/mL) + LPS (1 µg/mL); and IL-4 (20 ng/mL) for 24 h followed by LPS (1 µg/mL) for 24 h. Untreated BV2 cells were used as a control. Post-incubation, the supernatants were collected and levels of two pro-inflammatory cytokines, TNF-α and IL-6, were measured using the DuoSet ELISA Assay kit (R&D Systems, MN, USA). ELISA data was analyzed using GraphPad Prism 7.

RNA-sequencing and proteomics

Data for RNA-sequencing and proteomics in BMDMs were acquired and analyzed as mentioned previously (22).

Statistical analysis

One-way ANOVA was used for biological replicates. For each data point, triplicate biological replicates, each with triplicate technical replicates, were performed. Circadian rhythmicity was determined using ECHO analysis software. Statistical analyses were performed using GraphPad Prism 7 or Excel software (Microsoft).

Results

Expression of clock genes *Per2* and *Bmal1* in BV2 microglia follow a daily oscillation

Per2 and *Bmal1* are the best studied representatives of the positive and negative arm of the circadian transcriptional-translational feedback loop with predictable relationship (19, 20). They have been extensively studied in BV2 microglia, and hence, were employed as indicators of clock activity (41–43). To investigate whether the clock was functional in the BV2 microglial cell line, *Per2* and *Bmal1* gene expression were quantified in naïve (resting) BV2 microglial cells. To assess transcriptional levels of both clock genes, samples were collected starting at 16 h post-serum shock (Hours Post Serum Shock 16 or HPS16), every 2 h for 24 h (Figure 1A). Total RNA was isolated from each sample, and *Per2* and *Bmal1* transcript levels were measured using RT-qPCR. The Extended Circadian Harmonic Oscillator (ECHO) application (40) was used to identify oscillations in the transcriptional data and determine whether the gene products oscillated with a circadian period. The ECHO algorithm uses an extended solution of the fixed amplitude oscillator that incorporates the amplitude change coefficient and provides detailed information on the nature of circadian oscillations (40). ECHO analysis indicated that both *Per2* (ECHO period = 16 h, ECHO p-value = 8.31 x 10^{-13}) (Figure 1B) and *Bmal1* (ECHO period = 16 h, ECHO p-value = 1.11 x 10^{-10}) (Figure 1C) displayed oscillations at the transcriptional level, although these oscillations are shorter than those considered to be circadian. Both *Per2* and *Bmal1* mRNA oscillations had peaks at around HPS20 and HPS36 post serum shock and a trough around HPS28, paralleling what has been seen in other studies of BV2 microglia (41, 42). To further analyze the circadian clock components in BV2 microglia, Western blotting was performed using anti-PER2 and anti-BMAL1 antibodies over circadian time to quantify protein levels (Figure 1D). Both PER2 (Figure 1E) (ECHO period = 16 h, ECHO p-value = 2.7 x 10^{-8}) and BMAL1 (Figure 1F) (ECHO period = 16 h, ECHO p-value =1.3 x 10^{-4}) displayed significant oscillations according to ECHO with periods and phases that corresponded to what was noted for these genes at the transcript level.
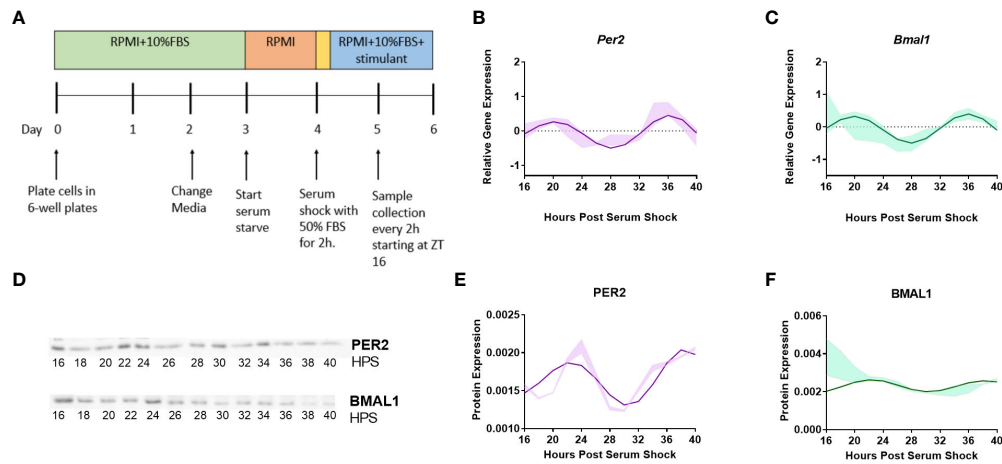
FIGURE 1

Clock genes *Per2* and *Bmal1* display circadian oscillations in resting BV2 microglia. **(A)** BV2 microglia were synchronized using the serum-shock protocol and samples were collected every 2 h starting at 16 h post serum-shock (HPS16) for RT-qPCR and Western blotting experiments. **(B, C)** ECHO fitted plots for mRNA expression of clock genes *Per2* and *Bmal1* in BV2 microglia. Data represented as fold change in expression using *Hprt1* as a reference gene and HPS0 as a reference sample for the ΔΔCt method of data analysis (n = 3) **(D)** Time course samples obtained from serum-shock synchronized BV2 cells analyzed using Western blotting to measure the levels of PER2 and BMAL1. Amido black staining was used to normalize for protein loading. For complete blot images refer to Supplementary Information (Supplementary Figures 3, 4) **(E, F)** ECHO fitted plots for PER2 and BMAL1 protein levels in BV2 cells (n = 3). For all ECHO plots, the bold lines depict the ECHO fitted model and the shaded region represents ±1 standard deviation of model at each time point. Statistical significance was determined using ECHO. All plots had p < 0.05 for ECHO significance fit.

The inflammatory status of the BV2 cell line affects the nature of clock protein oscillations

A functional circadian clock in bone-marrow derived mouse macrophages is receptive to the inflammatory state of the cells (31). Specifically, the activation of bone-marrow derived macrophages into a pro-inflammatory phenotype using LPS, TNF-α, or IFN-γ suppressed the oscillation of core clock components *Per2* and *Nr1d1*, whereas anti-inflammatory activation using IL-4 enhanced their expression (31). To assess whether a similar result is observed in microglia, we subjected BV2 cells to both pro- and anti-inflammatory activation. The bacterial endotoxin LPS, and the cytokine IL-4 have been successfully used in previous work and are known to be the strongest polarizing stimulants to activate BV2 microglia. Hence, LPS and IL-4 were used to activate BV2 microglia into pro- and anti-inflammatory states, respectively (44–52). Therefore, to evaluate the influence of LPS exposure on the circadian clock in BV2 microglia, BV2 cells were synchronized using serum-shock, and LPS (1 μg/mL) was added to the growth media post serum-shock. Time course samples for RT-qPCR analysis were collected every 2 h for 24 h starting at HPS16. We found that LPS exposure suppressed the oscillation of the clock genes *Per2* and *Bmal1* in BV2 microglia (Figure 2A). This loss of rhythm in the expression of the positive and negative arm components of the circadian feedback loop indicates that the pro-inflammatory activation of BV2 microglia has a suppressive effect on the circadian system, paralleling what was observed in primary macrophages (31).

The effect of the activation of BV2 microglia into the anti-inflammatory phenotype was assessed by exposing the BV2 cell line to IL-4 (20 ng/mL) after the BV2 cells were synchronized using serum-shock. As with LPS exposure, time course samples for RT-

qPCR analysis were collected every 2 h for 24 h starting at HPS16. Unlike for LPS addition, the expression of *Per2* (ECHO period = 16 h, ECHO p-value = 1.04 x 10^{-15}) and *Bmal1* (ECHO period = 16 h, ECHO p-value = 2.62 x. 10^{-13}) remained oscillatory (Figure 2B) following exposure to IL-4. However, the characteristics of the oscillation of *Per2* and *Bmal1* changed in response to the addition of IL-4. Compared to the resting state, upon IL-4 exposure both *Per2* and *Bmal1* underwent a phase inversion, with a peak around HPS24 to 28 and HPS28 to 32 respectively in the IL-4 activated microglia, as opposed to the peak at around HPS20 for both the genes in the resting state (compare Figures 1, 2). This change in the oscillatory behavior of IL-4 activated BV2 cells vs. resting cells, however, does not abrogate the retention of a daily oscillation in the anti-inflammatory state.

The BV2 microglial circadian clock times the expression of the NOX2 subunits p47^{phox} and gp91^{phox}

A hallmark of a cellular pro-inflammatory state is the presence of oxidative stress, as reflected in the production of ROS (9, 53). NOX2 is a major contributor to ROS production leading to oxidative stress (11, 15, 32, 54–57). With the known connection between the clock and inflammation, we hypothesized the circadian clock may control *Nox2* gene expression in BV2 microglia. NOX2 is comprised of six subunits, with gp91^{phox} and p22^{phox} serving as integral membrane proteins that together form the large heterodimeric subunit flavocytochrome b$_{558}$ (cytb$_{558}$) (58), and p40^{phox}, p47^{phox}, p67^{phox}, and Rac together forming the cytosolic subunits (55). Activation of NOX2 occurs though a complex series of protein-protein interactions and translocation (59, 60) driven by phosphorylation of p47^{phox}, which results in attachment of phospho-p47^{phox} to the p22^{phox} component of cytb$_{558}$, thus
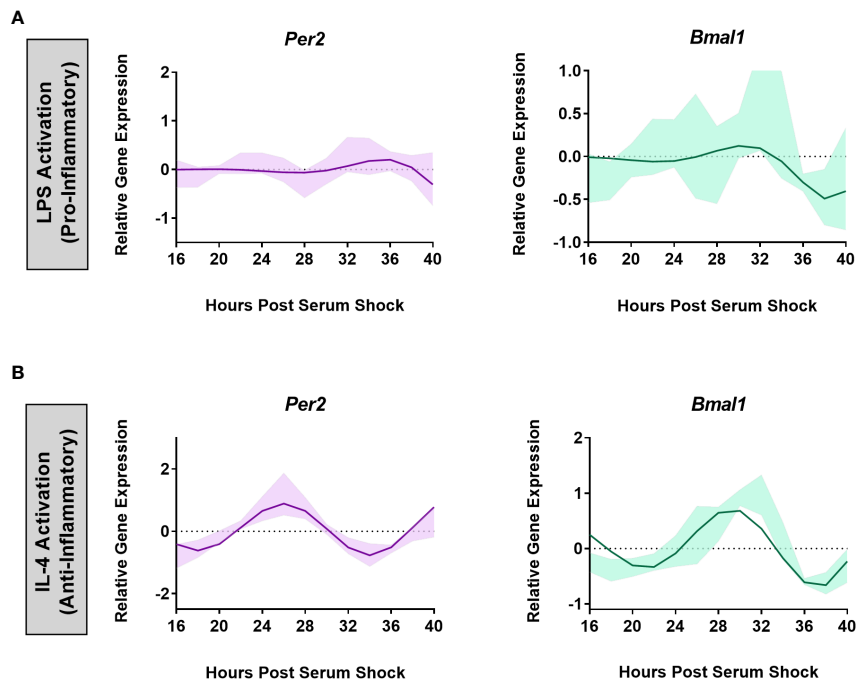
FIGURE 2
BV2 circadian clock oscillations are affected by the cell's inflammatory status. ECHO fitted plots for mRNA expression of clock genes *Per2* and *Bmal1* in BV2 microglia (n = 3) under **(A)** LPS (1 µg/mL) (pro-inflammatory) and **(B)** IL-4 (20 ng/mL) (anti-inflammatory) activation. Data represented as fold change in expression using *Hprt1* as a reference gene and HSP0 as a reference sample for the ΔΔCt method of data analysis. Bold line represent model fit with shaded region representing the standard deviation of model at each time point. All plots had p<0.05 for ECHO significance fit.

forming an active enzyme complex. For this study, we focused on two essential sub-units of NOX2; p47^{phox} and gp91^{phox} (11).

To assess whether gene expression of *p47^{phox}* and *gp91^{phox}* was under circadian control in BV2 microglia, time course samples were collected every 2 h for 24 h post-HPS16 from serum-shock synchronized BV2 cells and RT-qPCR was used to measure the expression of *p47^{phox}* and *gp91^{phox}*. In the resting state, both *p47^{phox}* (ECHO period = 16 h, ECHO p-value = 1.7 x 10^{-11}) and *gp91^{phox}* (ECHO period = 16 h, ECHO p-value = 1.3 x 10^{-17}) displayed significant oscillations, matching the oscillations in *Per2* and *Bmal1* (Figure 3A). ECHO plots for both subunits showed peaks around HPS20-24 and HPS36-40, and a trough around HPS28-32, paralleling what was seen for *Per2* and *Bmal1* in the resting state in BV2 cells.

It is known that NOX2 is activated upon addition of LPS (61). Given what we found relating to the effect of LPS on the clock in BV2 microglia, we next assessed the effect of LPS on NOX2 component oscillations. The addition of 1 µg/mL LPS after serum synchronization resulted in the loss of circadian oscillations in both *p47^{phox}* and *gp91^{phox}* transcript levels (Figure 3B). Conversely, the addition of 20 ng/mL IL-4 after serum synchronization did not result in a loss of circadian oscillations for either *p47^{phox}* (ECHO period = 16 h, ECHO p-value = 4.98 x 10^{-7}) or *gp91^{phox}* (ECHO period = 16 h, ECHO p-value = 1.57 x 10^{-6}) (Figure 3C). Interestingly, there was again a shift in phase between the resting and IL-4 activated states, paralleling what was seen in *Per2* and *Bmal1* after the addition of IL-4. *p47^{phox}* expression underwent a phase inversion, with a peak at HPS28-32, as compared to a peak at HPS20 in the resting state. Thus, the two key NOX2 subunits are under circadian regulation in BV2 microglia.

NOX2 inhibition supports a role for NOX2 in the circadian inflammatory response of BV2 microglia

Given the oscillation of NOX2 and the loss of circadian gene expression both in clock and *Nox2* genes in the pro-inflammatory state, we hypothesized there was a role for NOX2 in clock-driven inflammation. To validate this role for NOX2 in circadian-driven inflammation, we next assessed the effect of NOX2 inhibitors on oscillations in the core clock gene transcripts as well as NOX2 gene expression. To do so, we employed two NOX2 inhibitors to suppress NOX2 function – apocynin (4-hydroxy-3-methoxy-acetophenone) (62–64) and GSK2795039 (GSK, N-(1-Isopropyl-3-(1-methylindolin-6-yl)-1H-pyrrolo[2,3-b]pyridin-4-yl)-1-methyl-1H-pyrazole-3-sulfonamide) (65). Apocynin is known to block the translocation of p47^{phox} to the membrane and its interaction with membrane-bound p22^{phox}, thereby preventing the formation of the active enzyme complex (66). Apocynin in not NOX2 specific but is used indiscriminately as a broad NOX inhibitor (67). GSK is a competitive reversible inhibitor of NADPH binding to cytb$_{558}$ *in vitro* and *in vivo* (65), and is selective for NOX2 as compared to the other NOX isoforms, xanthine oxidase, and endothelial nitric oxide synthase (65).

As a proxy for the activity of NOX2 in the presence of LPS and inhibitors, we determined ROS levels *via* Amplex Red (extracellular) and DCFDA (intracellular) assays. For both assays, additives such as LPS, apocynin or GSK were introduced to serum-shock synchronized BV2 at HPS20 and ROS was measured upon exposure of the BV2 cells to LPS only, LPS with either apocynin or GSK, or no additive
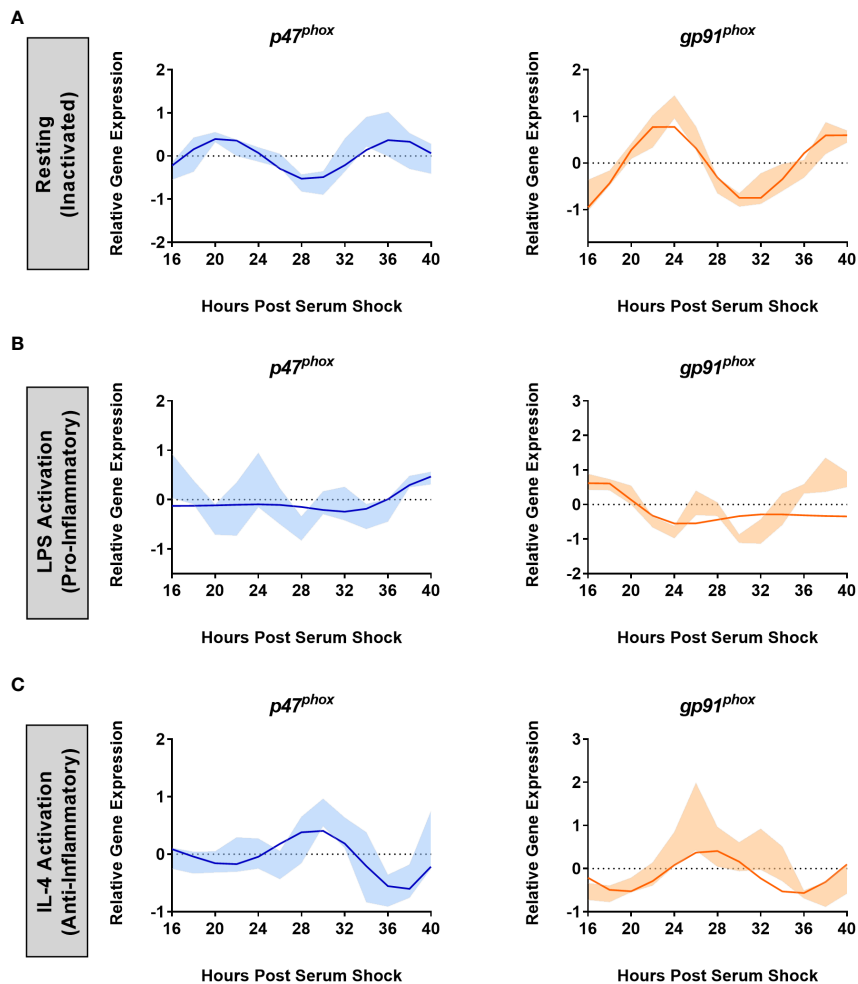
FIGURE 3

NOX2 sub-units *p47^phox* and *gp91^phox* are under the control of the BV2 microglial circadian clock. ECHO fitted plots for mRNA expression of NOX2 components *gp91^phox* and *p47^phox* in BV2 microglia (n = 3) under **(A)** resting, **(B)** LPS (1 µg/mL) (pro-inflammatory) and **(C)** IL-4 (20 ng/mL) (anti-inflammatory) activation. Data represented as fold change in expression using *Hprt1* as a reference gene and HSP0 as a reference sample for the ΔΔCt method of data analysis. Bold line represent model fit with shaded region representing the standard deviation of model at each time point. All plots had p < 0.05 for ECHO significance fit.

(control) for 2 h. In the presence of LPS, both extra- and intracellular ROS levels in BV2 microglia increased relative to the control (Figures 4A, B). In the absence of LPS, neither apocynin nor GSK influenced the levels of ROS produced (Figures 4A, B). However, in the presence of both LPS and either apocynin or GSK, the levels of both extra- and intracellular ROS were significantly reduced relative to the presence of LPS alone, and were even significantly lower than the control (Figures 4A, B). These results suggest that the inhibition of NOX2 may prevent ROS production in BV2 microglia as compared to even basal levels as well as in the presence of LPS.

A key step in the activation of NOX2 is the phosphorylation of the p47^phox subunit (55). To confirm that inhibition of ROS levels by apocynin was NOX2 dependent, even in the presence of LPS, Western blots were obtained to quantify levels of phospho-p47^phox upon LPS and apocynin addition (Figure 4C). Given that traditionally used loading controls, such as GAPDH and β-Actin, are under the control of the circadian clock, Amido Black staining was used as an internal loading control to measure total protein loaded in a lane and normalize protein levels (68). In the presence of LPS, there was a 40% increase in phospho-p47^phox levels. In the presence of LPS + apocynin, however, levels of phospho-p47^phox fell to approximately 15% below that of the control. These results correlated with extracellular ROS levels (Figures 4A, B). The reduction in phospho-p47^phox levels in the presence of LPS + apocynin suggests that apocynin might regulate ROS production upstream of p47^phox phosphorylation (69–71). Interestingly, when we repeated the experiment with LPS + GSK, we found that GSK did not affect phospho-p47^phox levels (Figure 4C), which was not unexpected as GSK inhibits the NOX2 cytochrome downstream of the phospho-p47^phox membrane translocation. Overall, these results confirm effective reduction in ROS levels due to microglial pro-inflammatory activation through the inhibition of NOX2 in the presence of apocynin or GSK, suggesting that NOX2 is the primary source of ROS in BV2 microglia.

Having established that BV2 cells express an active NOX2 that is inhibited by apocynin and GSK, we next studied the effect of NOX2 inhibition on clock gene expression to validate a role for NOX2 in clock-driven inflammation. Serum-shock synchronized BV2 cells
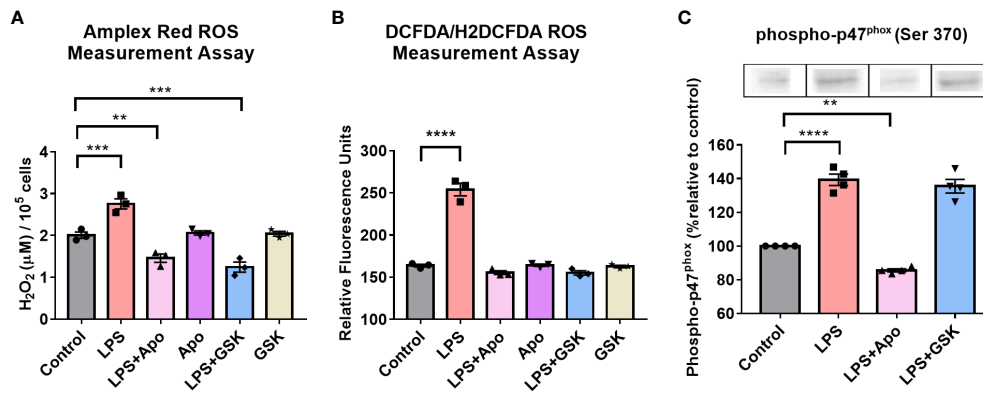
FIGURE 4
NOX2 inhibition in BV2 microglia results in the reduction of ROS levels and affects phosphorylated-p47^{phox} levels. ROS levels in BV2 microglia with and without LPS and, NOX2 inhibitors apocynin and GSK2795039 determined using **(A)** Amplex Red Assay to measure extracellular hydrogen peroxide levels and **(B)** DCFDA Assay to measure intracellular ROS levels. **(C)** Western blotting analysis of phosphorylated-p47^{phox} levels in BV2 microglia in the presence of LPS and NOX2 inhibitors apocynin and GSK2795039 (n = 3 to 4). For all experiments, BV2 cells with no additives were used as control sample. Data are represented as mean $\pm$ SEM and analyzed using single-factor ANOVA test. ** denotes p<0.01, **** denotes p<0.0001 and *** denotes p<0.001. For complete blot images, refer to Supplementary Information (Supplementary Figure 5).

were exposed to LPS (1 µg/mL) in the presence of apocynin (100 µM) or GSK (25 µM). Time course samples were collected every 2 h for 24 h starting at HPS16. Addition of apocynin under LPS activation rescued the oscillations in *Per2* (ECHO period = 16 h, ECHO p-value = 1.17 x 10^{-6}) and *gp91^{phox}* (ECHO period = 16 h, ECHO p-value = 1.03 x 10^{-12}), which showed oscillations consistent with naïve BV2 microglia (Supplementary Figures 1A, D). Conversely, *Bmal1* and *p47^{phox}* expression levels no longer showed significant oscillations

(Supplementary Figures 1B, C). However, the addition of LPS + GSK rescued oscillations in all four genes: *Per2* (ECHO period = 16 h, ECHO p-value = 2.06 x 10^{-12}), *Bmal1* (ECHO period = 16 h, ECHO p-value = 1.02 x 10^{-17}), *p47^{phox}* (ECHO period = 16 h, ECHO p-value = 5.46 x 10^{-5}) and *gp91^{phox}* (ECHO period = 16 h, ECHO p-value = 1.48 x 10^{-10}), displaying oscillations consistent with naïve BV2 macrophages at the transcriptional level (Figure 5). This retention of oscillations under NOX2 inhibition, particularly with GSK,
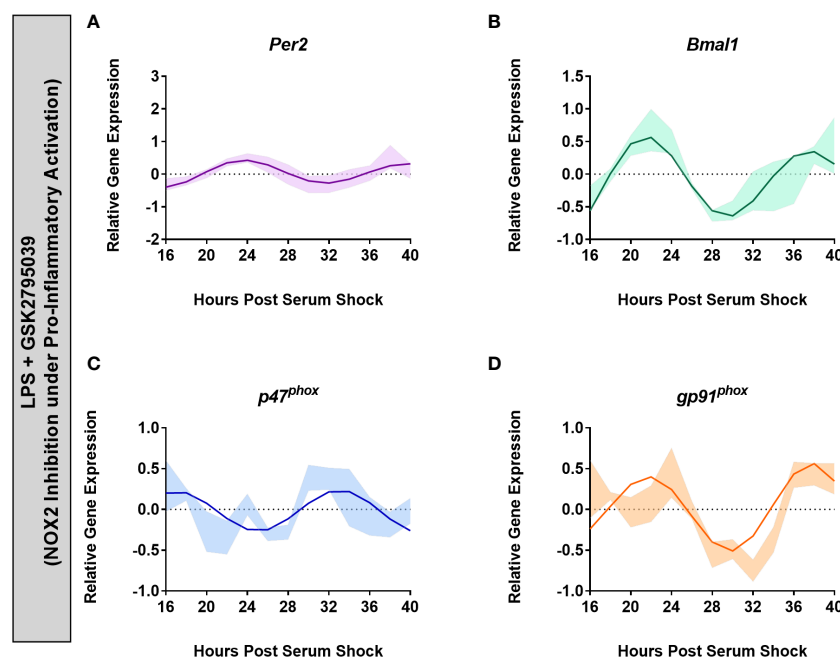
FIGURE 5
Inhibition of NOX2 by GSK2795039 under LPS activation results in the retention of circadian oscillations in BV2 microglia. ECHO fitted plots for mRNA expression of clock genes (n = 3) **(A)** *Per2* and **(B)** *Bmal1*, and NOX2 components **(C)** *gp91^{phox}* and **(D)** *p47^{phox}* in BV2 microglia in the presence of 1 µg/mL LPS and 25 µM GSK2795039. Data represented as fold change in expression using *Hprt1* as a reference gene and HSP0 as a reference sample for the ΔΔCt method of data analysis. Bold line represent model fit with shaded region representing the standard deviation of model at each time point. All plots had p<0.05 for ECHO significance fit.

suggests that NOX2 might play a circadian regulatory role in BV2 microglia by facilitating the transition into a pro-inflammatory phenotype.

NOX2 regulates the circadianly-induced transition of bone-marrow derived macrophages into a pro-inflammatory state

To validate that the results obtained in BV2 microglia were consistent in primary cells, we next studied the effect of NOX2 inhibition on the circadian clock in bone marrow-derived macrophages (BMDMs). We searched our previous quantitative RNA-sequencing and proteomic analysis datasets (22) to assess the oscillation of $p47^{phox}$ and $gp91^{phox}$ in BMDMs. At the transcriptional level, *Per2* (ECHO period = 23.1 h, ECHO p-value = 3.89 x 10^{-20}) and *Bmal1* (ECHO period = 29.3 h, ECHO p-value = 3.96 x 10^{-20}) showed significant oscillation along with $p47^{phox}$ (ECHO period = 19.5 h, ECHO p-value = 1.37 x 10^{-4}), though $gp91^{phox}$ had an oscillation beyond the circadian range (ECHO period = 36 h, ECHO p-value = 6.82 x 10^{-8}) (Supplementary Figure 2A). However, analysis of the proteomic dataset revealed that along with PER2 protein levels (Figure 6A), BMAL1 (ECHO period = 28.9 h, ECHO p-value = 1.32 x 10^{-5}), and $gp91^{phox}$ (ECHO period = 19.7 h, ECHO p-value =

6.76 x 10^{-5}) oscillated with a circadian period, suggesting the post-transcriptional circadian regulation of $gp91^{phox}$, which is common in murine macrophages (Supplementary Figure 2B) (22).

To assess the role of NOX2 inhibition on the circadian clock in BMDMs, we used luciferase luminescence measurements to track the levels of PER2 in real time. For this, *Per2::Luc* mice, in which a *Luc* gene is fused in-frame to the 3' end of the endogenous *mPer2* gene, was used (72). This targeted reporter results in the expression of PER2::LUC bioluminescence similar to endogenous *Per2* expression, rendering it as a real-time reporter of circadian dynamics (72). Bone marrow progenitor cells extracted from *Per2:Luc* C57BL/6J mice were differentiated with recombinant M-CSF into BMDMs and serum-shock synchronized, as per a previously established protocol (22, 39). PER2::LUC bioluminescence in BMDMs was assayed over several days using a LumiCycle32 with Leibovitz media containing Luciferin (22, 39). Samples treated with neither LPS nor NOX2 inhibitors added were used as controls to confirm that PER2 protein levels oscillated with a circadian period in *Per2:Luc* BMDMs (Figures 6A, B). We next treated these BMDMs with either LPS (1 µg/mL) or IL-4 (20 ng/mL) post-serum shock, as we did with the BV2 microglia, to elicit pro- and anti-inflammatory activation in the BMDMs respectively. We also analyzed the effect of LPS with NOX2 inhibitors (apocynin (100 µM) and GSK (25 µM)) on PER2 levels in BMDMs. When LPS and/or NOX2 inhibitors were added to the BMDMs post serum-shock
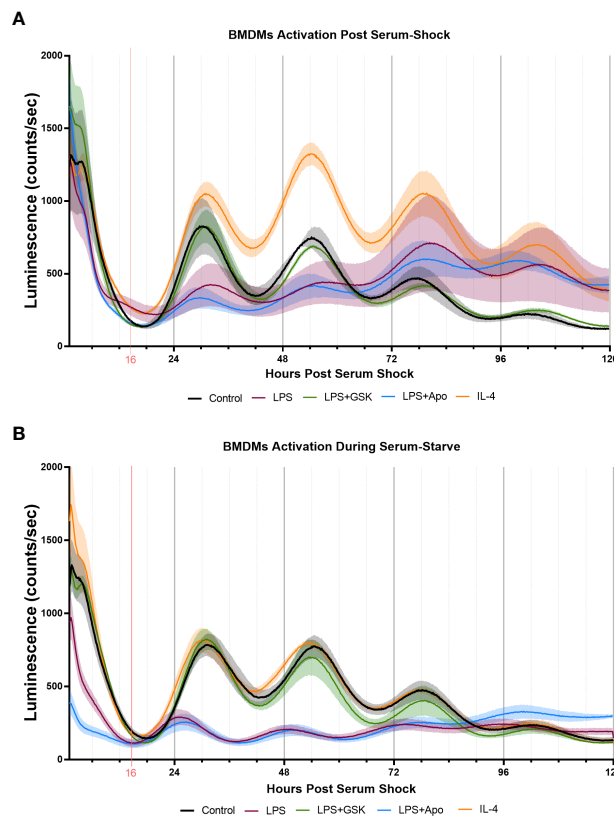
FIGURE 6
Inhibition of NOX2 by GSK2795039 under LPS activation conserves PER2 oscillation in mouse bone marrow-derived macrophages (BMDMs). Luminescence traces obtained luciferase measurement of serum-shock synchronized mouse BMDMs with and without LPS, and NOX2 inhibitors.
(A) Cells were exposed to LPS with and without NOX2 inhibitors apocynin and GSK2795039 during the starve stage of the synchronization protocol.
(B) Cells were exposed to LPS with and without NOX2 inhibitors apocynin and GSK2795039 post serum-shock stage of the synchronization protocol. Luciferase measurements were obtained by the LumiCycle HPS0 to HPS120 (n = 3). Data are represented as mean ± SEM.

synchronization, LPS resulted in a reduction of PER2 amplitude compared to the control sample (Figure 6A). When apocynin was added in parallel with LPS, there was a similar decrease in the amplitude of the PER2 oscillation. However, samples in which GSK was added in parallel with LPS maintained the amplitude in PER2 oscillations as compared to untreated BMDMs (Figure 6A). Conversely, IL-4 addition resulted in an increase in the amplitude of the PER2 oscillation as compared to the control sample.

Unlike what we had carried out with BV2 microglia, previous work on the response of PER2 oscillations in BMDMs to immunological challenge was performed by adding the treatment prior to serum shock (31). Therefore, to mimic this approach, we repeated our assay of PER2 oscillations in BMDMs by treating the cells with immune insults prior to serum shock synchronization. Like what was seen in BV2 microglia and in post serum shock exposure, exposure to IL-4 did not affect PER2 oscillations as compared to the control sample (Figure 6B). When added prior to serum synchronization, LPS addition resulted in the reduction of PER2 levels overall, as well as a reduction in the amplitude of the PER2 oscillation, as has been previously reported (Figure 6B) (31). When apocynin was added in combination with LPS prior to serum synchronization, the reduction in PER2 levels and amplitude of oscillation was conserved (Figure 6B). However, when GSK was added in combination with LPS prior to serum synchronization, PER2 levels and oscillations were similar to that of the control (Figure 6B). The ability of GSK to rescue the levels and amplitude of oscillation of PER2 in BMDMs during LPS activation is consistent

with our results in BV2 microglia, and further suggests that NOX2 might play a regulatory role in the circadianly-regulated transition of cells from the monocyte lineage into a pro-inflammatory state.

Effect of NOX2 on the pro-inflammatory profile of BV2 microglia and BMDMs

To further profile the role of NOX2 in the pro-inflammatory activation of BV2 microglia and BMDMs, we quantified the expression of two common inflammatory cytokines, TNF-α and IL-6, in response to LPS treatment with and without NOX2 inhibitors. Serum-synchronized BV2 cells were stimulated using LPS (1 μg/mL) with and without apocynin (100 μM) or GSK (25 μM) at HPS20. We chose HPS20 as a time point both to allow sufficient time for the cells to recover from the serum-shock, to avoid artifactual gene expression that occurs immediately following serum-shock (37), and to overlap with the peak time in *Per2* oscillation as observed in inactivated BV2 microglia (Figure 1B). After 24 h incubation starting at HPS20, the supernatant was collected from BV2 microglia and TNF-α and IL-6 levels were measured using ELISA (Figures 7A, B). BV2 microglia treated with LPS demonstrated a significant increase of both TNF-α and IL-6 compared to untreated cells. BV2 microglia treated with only apocynin, or GSK showed no significant change in TNF-α and IL-6 levels compared to untreated cells. However, when apocynin or GSK was added individually in parallel with LPS treatment, there was a significant reduction in TNF-α and IL-6 levels relative to samples
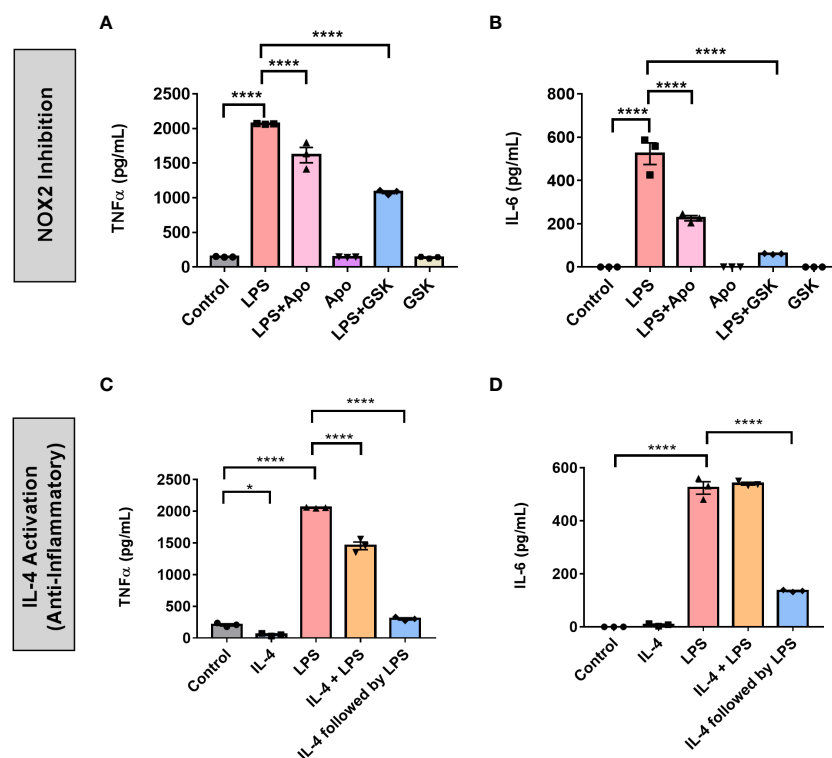
FIGURE 7
NOX2 inhibition in BV2 microglia creates an inflammatory environment similar to anti-inflammatory activation. **(A)** TNF-α and **(B)** IL-6 (pro-inflammatory cytokines) levels in BV2 cells (n = 3) with and without LPS and NOX2 inhibitors apocynin and GSK2795039 measured using ELISA. **(C)** TNF-α and **(D)** IL-6 (pro-inflammatory cytokines) levels in BV2 cells (n = 3) under IL-4 activation with and without LPS measured using ELISA. Data are represented as mean $\pm$ SEM and analyzed using single-factor ANOVA test. * denotes $p < 0.05$ and **** denotes $p < 0.0001$.

with LPS treatment alone, with the greatest reduction in cytokine levels observed in the GSK-treated cells.

We next compared NOX2 inhibition to the anti-inflammatory effect on cytokine production in BV2 microglia. To this end, we assessed the effect of IL-4 activation on TNF-α and IL-6 production in BV2 microglia (Figures 7C, D). Serum synchronized BV2 cells were incubated with IL-4 (20 ng/mL) for 24 h starting at HPS20. After a 24 hr incubation with IL-4, the media was replaced with fresh media containing LPS (1 μg/mL). In addition, we treated serum synchronized BV2 cells with LPS and IL-4 simultaneously or individually and incubated the cells for 24 h starting at HPS20. While TNF-α levels showed a slight, albeit significant, drop in levels in the presence of IL-4 (Figure 7C), no significant change in IL-6 levels was observed (Figure 7D). Co-treatment of LPS and IL-4 resulted in significant reduction of TNF-α levels compared to samples that had only LPS, IL-6 levels remained unchanged (Figure 7D). Interestingly, LPS activation of BV2 cells post-24 h incubation with IL-4 resulted in a significant drop of both TNF-α and IL-6 (Figures 7C, D).

We repeated these experiments in BMDMs to study the effect of NOX2 inhibition on pro-inflammatory activation in primary cells. Serum shock synchronized BMDMs were stimulated using LPS (1 μg/mL) with and without apocynin (100 μM) or GSK (25 μM) at HPS20. After a 24 h incubation, the supernatant was collected and TNF-α and IL-6 levels were measured using ELISA (Figures 8A, B). BMDMs treated with LPS demonstrated a significant increase in TNF-α and IL-6 levels compared to the untreated control (Figures 8A, B). Concordant with what was seen in BV2 cells, NOX2 inhibition by either apocynin or GSK during LPS treatment resulted in a significant reduction in both TNF-α and IL-6 levels as compared to BMDMs exposed only to LPS. While LPS + GSK showed a more significant drop in TNF-α and IL-6 levels than LPS + apocynin in BV2 microglia, such a difference was not observed in the BMDMs. Compared to BMDMs treated with LPS, addition of IL-4 along with LPS resulted in lower levels of IL-6 (Figure 8B). Interestingly, addition of apocynin or GSK along with LPS resulted in the secretion of significant amounts of IL-4 in BMDMs compared to naïve BMDMs or BMDMs exposed

only to LPS (Figure 8C). Comparison of ELISA results from IL-4 activation (Figures 7C, D) and NOX2 inhibition (Figures 7A, B) in BV2 microglia and that of mouse BMDMs (Figure 8) suggests that inhibiting NOX2 leads to a microglial response that is similar to that of an anti-inflammatory activation. This is consistent with the inhibition of NOX2 using GSK, wherein the circadian clock retained its oscillation for all genes of interest. These results taken together might indicate that NOX2 inhibition leads to an anti-inflammatory response from both microglia and macrophages, which results in the conservation of circadian oscillations even upon pro-inflammatory activation.

Discussion

The internal circadian clock comprises a transcription/translation negative feedback loop (TTFL) that controls physiology in macrophages and monocytes to regulate the immune response, playing an important role in the regulation of inflammation, glial activation, oxidative stress, and autophagy (18, 24). Concordantly, circadian clock dysfunction has been found to have direct implications on the progression of inflammation, redox defense, and cell death (18). While several studies have been directed towards understanding the impact of circadian regulation on peripheral macrophages, relatively few have focused on microglia. We observed that *Per2* and *Bmal1* gene expression, and PER2 and BMAL1 protein production in serum-shock synchronized BV2 cells displayed circadian oscillations at both transcriptional and protein levels (Figure 1). Studies beyond our own have shown that *Per1, Per2, Rev-erb* and *Bmal1* display rhythmic expression, but like our study, have found that while they are predicted to oscillate with a 24 h period in an anti-phasic pattern, this is not the case in the BV2 microglial line (Figure 1) (21–23). We predict this is likely due to the circadian modulatory effects commonly noted in cell lines (41, 42).

While the effect of the microglial circadian clock on its immune response has been studied (24, 42, 73–75), the effect of microglial phenotypes on the circadian clock has not been investigated. Pro-
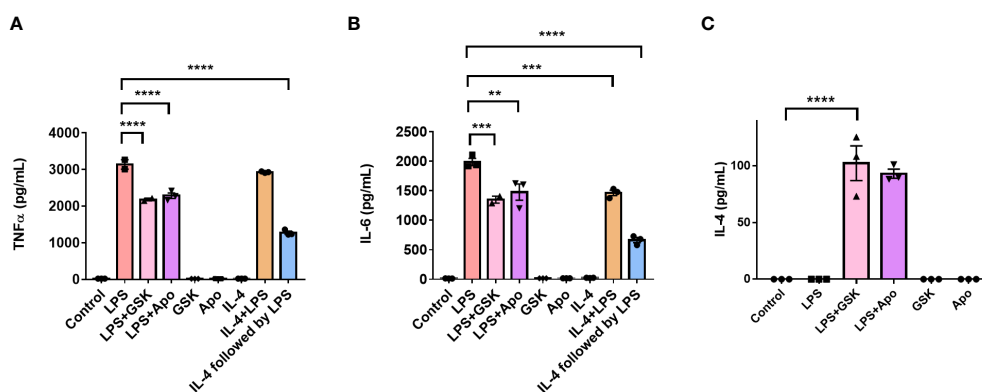
FIGURE 8
NOX2 inhibition affects the levels of inflammation associated cytokines in mouse bone marrow-derived macrophages. **(A)** TNF-α and **(B)** IL-6 (pro-inflammatory cytokines), and **(C)** IL-4 (anti-inflammatory cytokine) levels in BMDMs (n = 3) with and without LPS and NOX2 inhibitors apocynin and GSK2795039 measured using ELISA. Based on ELISA data, we did not see any IL-4 secretion from BV2 microglia. This could be because of the immortalization process. Data are represented as mean ± SEM and analyzed using single-factor ANOVA test. ** denotes p < 0.01, *** denotes p < 0.001 and **** denotes p < 0.0001.

inflammatory activation of primary macrophages suppresses *Per2* oscillations, whereas anti-inflammatory activation results in *Per2* amplification (31). We observed similar results for BV2 microglia, wherein the cells lost circadian rhythmicity in *Per2* and *Bmal1* expression upon exposure to LPS (Figure 2A) but retained circadian oscillations upon IL-4 exposure (Figure 2B). This suggests that BV2 microglia respond in a similar manner to macrophages and that there is a strong dependence of the microglial clock on the cellular inflammatory state.

Oxidative stress resulting from macrophages or microglial activation is under circadian control (36, 76). NOX4 in aortic endothelial cells is influenced by the circadian rhythm (77) and the inhibition of superoxide ameliorated LPS-induced changes in circadian periodicity in peritoneal macrophages (78). NOX2 is associated with the progression of various neurodegenerative diseases (14, 17, 32, 54, 79–84). Notably, the inhibition of NOX2 in vascular endothelial cells using diphenyleneiodonium chloride (DPI) restored PER2 rhythmicity under LPS stimulation (85). While these findings linked the circadian clock and oxidative stress, we have shown herein that gene expression of $p47^{phox}$ and $gp91^{phox}$ are timed by the clock, indicating that NOX2 is directly timed by the microglial circadian clock. Moreover, we demonstrated that the inflammatory state of the cell has a direct effect on the oscillatory expression of both $p47^{phox}$ and $gp91^{phox}$ (Figure 3).

While it is clear that NOX2 is controlled by the clock, the reciprocal effect of NOX2 on the clock was unknown. We demonstrated that NOX2 inhibition, by apocynin or GSK, resulted in significant reduction in ROS production and $p47^{phox}$ phosphorylation when BV2 cells were activated with LPS (Figure 4). Importantly, GSK also rescued rhythmic expression of the two clock genes and two NOX2 genes being tracked (Figure 5). This may indicate that NOX2 plays a crucial role in the transition of microglia from a resting state into a pro-inflammatory phenotype. In parallel, previous studies have shown that $p47^{phox}$ knockout mice and apocynin-treated mice display reduced levels of cerebrovascular dysfunction and ROS, and increased anti-inflammatory activation of microglia (86). Combined with our data, this suggests that NOX2 may facilitate the link between the circadian recognition of the pro-inflammatory microglial phenotype during neuroinflammation (14).

The results observed in BV2 microglia were further supported by trends obtained in primary mouse BMDMs, with clear oscillations in the levels of $gp91^{phox}$ and $p47^{phox}$. The rescue of PER2 by GSK during LPS treatment directly paralleled what we observed in BV2 microglia (Figure 6). Of note, apocynin failed to improve the amplitude of PER2 oscillations in the presence of LPS. Furthermore, inhibition of NOX2 by apocynin and knockouts of *Nox2* have been shown to reduce pro-inflammatory microglial phenotypes (81). Concordantly, we observed that TNF-α and IL-6 production was significantly reduced in BV2 cells when either apocynin or GSK were present with LPS (Figures 7A, B). These results paralleled the reduction in levels of TNF-α and IL-6 as a result of IL-4 priming (i.e., incubated with IL-4 for 24 h) prior to exposure to LPS (Figures 7C, D). Similar results were observed when TNF-α and IL-6 levels were measured in BMDMs under NOX2 inhibition, with both cytokines significantly reduced in the presence of GSK along with LPS (Figures 8A, B). IL-4 levels significantly

increased when NOX2 was inhibited using apocynin or GSK in the presence of LPS (Figure 8C) indicating that NOX2 inhibition might create a microglial response similar to that of anti-inflammatory activation by IL-4. This could explain why creation of such an anti-inflammatory environment supports retention of the circadian clock in BV2 even in the presence of LPS (Figures 5, 6).

In summary, although neuroinflammation and circadian disruption have been attributed to be major drivers of various neurodegenerative diseases (27), their interrelationship remains unclear. We observed that the BV2 circadian clock depends on the nature of activation of BV2 cells. Furthermore, inhibiting NOX2 resulted in the maintenance of the circadian clock even under pro-inflammatory activation. We suggest that NOX2 is a critical regulator of the microglial inflammatory state and circadian clock function. NOX2 inhibition under pro-inflammatory activation results in the retention of a functional circadian clock in microglia by regulating the inflammatory environment. Our work further suggests a strong link between NOX2 inhibition and the circadian clock in BV2 microglia and primary macrophages that could be further explored, for example in a neuroinflammation mouse model, in the development of therapeutics to target neuroinflammation.

Data availability statement

The original contributions presented in the study are included in the article/Supplementary Material. Further inquiries can be directed to the corresponding author.

Ethics statement

All animal procedures were approved by the Rensselaer Polytechnic Institute Animal Care and Use Committee (https://research.rpi.edu/compliance/oversight-committees/institutional-animal-care-and-use-committee#:~:text=Rensselaer's%20Institutional%20Animal%20Care%20and,use%20of%20animals%20in%20research.).

Author contributions

JD and JH supervised the project. IM designed and performed all the experiments. SB managed all mouse work and contributed to analysis of mouse data. IM wrote and edited the manuscript with input and revisions from JD and JH. All authors contributed to the article and approved the submitted version.

Funding

Acknowledgments

Conflict of interest

The authors declare that the research was conducted in the absence of any commercial or financial relationships that could be construed as a potential conflict of interest.

Publisher's note

All claims expressed in this article are solely those of the authors and do not necessarily represent those of their affiliated organizations, or those of the publisher, the editors and the reviewers. Any product that may be evaluated in this article, or claim that may be made by its manufacturer, is not guaranteed or endorsed by the publisher.

Supplementary material

The Supplementary Material for this article can be found online at: https://www.frontiersin.org/articles/10.3389/fimmu.2023.1106515/full#supplementary-material

References

1. Frank-Cannon TC, Alto LT, McAlpine FE, Tansey MG. Does neuroinflammation fan the flame in neurodegenerative diseases? *Mol Neurodegener* (2009) 4(1):1–13. doi: 10.1186/1750-1326-4-47

2. Crain JM, Nikodemova M, Watters JJ. Microglia express distinct M1 and M2 phenotypic markers in the postnatal and adult central nervous system in male and female mice. *J Neurosci Res* (2013) 91(9):1143–51. doi: 10.1002/jnr.23242

3. Kigerl KA, Gensel JC, Ankeny DP, Alexander JK, Donnelly DJ, Popovich PG. Identification of two distinct macrophage subsets with divergent effects causing either neurotoxicity or regeneration in the injured mouse spinal cord. *J Neurosci* (2009) 29 (43):13435–44. doi: 10.1523/JNEUROSCI.3257-09.2009

4. Boche D, Perry VH, Nicoll JAR. Review: Activation patterns of microglia and their identification in the human brain. *Neuropathol Appl Neurobiol* (2013) 39(1):3–18. doi: 10.1111/nan.12011

5. Walker DG, Lue LF. Immune phenotypes of microglia in human neurodegenerative disease: Challenges to detecting microglial polarization in human brains. *Alzheimers Res Ther* (2015) 7(1):1–9. doi: 10.1186/s13195-015-0139-9

6. Luo XG, Chen S. The changing phenotype of microglia from homeostasis to disease. *Transl Neurodegener* (2012) 1:1–13. doi: 10.1186/2047-9158-1-9

7. Chhor V, le Charpentier T, Lebon S, Oré MV, Celador IL, Josserand J, et al. Characterization of phenotype markers and neuronotoxic potential of polarised primary microglia in vitro. *Brain Behav Immun* (2013) 32:70–85. doi: 10.1016/j.bbi.2013.02.005

8. Ransohoff RM. A polarizing question: Do M1 and M2 microglia exist. *Nat Neurosci* (2016) 19(8):987–91. doi: 10.1038/nn.4338

9. Orihuela R, McPherson CA, Harry GJ. Microglial M1/M2 polarization and metabolic states. *Br J Pharmacol* (2016) 173(4):649–65. doi: 10.1111/bph.13139

10. Cherry JD, Olschowka JA, O'Banion MK. Neuroinflammation and M2 microglia: The good, the bad, and the inflamed. *J Neuroinflamm* (2014) 11:1–15. doi: 10.1186/1742-2094-11-98

11. Bedard K, Krause KH. The NOX family of ROS-generating NADPH oxidases: Physiology and pathophysiology. *Physiol Rev* (2007) 87(1):245–313. doi: 10.1152/physrev.00044.2005

12. Collin F. Chemical basis of reactive oxygen species reactivity and involvement in neurodegenerative diseases. *Int J Mol Sci* (2019) 20(10). doi: 10.3390/ijms20102407

13. Wilking M, Ndiaye M, Mukhtar H, Ahmad N. Circadian rhythm connections to oxidative stress: Implications for human health. *Antioxid Redox Signal* (2013) 19(2):192–208. doi: 10.1089/ars.2012.4889

14. Ma MW, Wang J, Zhang Q, Wang R, Dhandapani KM, Vadlamudi RK, et al. NADPH oxidase in brain injury and neurodegenerative disorders. *Mol Neurodegener* (2017) 12(1):1–28. doi: 10.1186/s13024-017-0150-7

15. Maghzal GJ, Krause KH, Stocker R, Jaquet V. Detection of reactive oxygen species derived from the family of NOX NADPH oxidases. *Free Radic Biol Med* (2012) 53 (10):1903–18. doi: 10.1016/j.freeradbiomed.2012.09.002

16. Cifuentes-Pagano E, Csanyi G, Pagano PJ. NADPH oxidase inhibitors: A decade of discovery from Nox2ds to HTS. *Cell Mol Life Sci* (2012) 69(14):2315–25. doi: 10.1007/s00018-012-1009-2

17. Surace MJ, Block ML. Targeting microglia-mediated neurotoxicity: The potential of NOX2 inhibitors. *Cell Mol Life Sci* (2012) 69(14):2409–27. doi: 10.1007/s00018-012-1015-4

18. Labrecque N, Cermakian N. Circadian clocks in the immune system. *J Biol Rhythms* (2015) 30(4):277–90. doi: 10.1177/0748730415577723

19. Roenneberg T, Merrow M. The circadian clock and human health. *Curr Biol* (2016) 26(10):R432–43. doi: 10.1016/j.cub.2016.04.011

20. Hurley JM, Loros JJ, Dunlap JC. Circadian oscillators: Around the transcription-translation feedback loop and on to output. *Trends Biochem Sci* (2016) 41(10):834–46. doi: 10.1016/j.tibs.2016.07.009

21. Keller M, Mazuch J, Abraham U, Eom GD, Herzog ED, Volk HD, et al. A circadian clock in macrophages controls inflammatory immune responses. *Proc Natl Acad Sci* (2009) 106(50):21407–12. doi: 10.1073/pnas.0906361106

22. Collins EJ, Cervantes-Silva MP, Timmons GA, O'Siorain JR, Curtis AM, Hurley JM. Post-transcriptional circadian regulation in macrophages organizes temporally distinct immunometabolic states. *Genome Res* (2021) 31(2):171–85. doi: 10.1101/gr.263814.120

23. Hayashi Y, Koyanagi S, Kusunose N, Okada R, Wu Z, Tozaki-Saitoh H, et al. The intrinsic microglial molecular clock controls synaptic strength *via* the circadian expression of cathepsin s. *Sci Rep* (2013) 3:1–7. doi: 10.1038/srep02744

24. Fonken LK, Frank MG, Kitt MM, Barrientos RM, Watkins LR, Maier SF. Microglia inflammatory responses are controlled by an intrinsic circadian clock. *Brain Behav Immun* (2015) 45:171–9. doi: 10.1016/j.bbi.2014.11.009

25. Hergenhan S, Holtkamp S, Scheiermann C. Molecular interactions between components of the circadian clock and the immune system. *J Mol Biol* (2020) 432 (12):3700–13. doi: 10.1016/j.jmb.2019.12.044

26. Durrington HJ, Farrow SN, Loudon AS, Ray DW. The circadian clock and asthma. *Thorax* (2014) 69(1):90–2. doi: 10.1136/thoraxjnl-2013-203482

27. Homolak J, Mudrovčić M, Vukić B, Toljan K. Circadian rhythm and alzheimer's disease. *Med Sci* (2018) 6(3):52. doi: 10.3390/medsci6030052

28. Segal JP, Tresidder KA, Bhatt C, Gilron I, Ghasemlou N. Circadian control of pain and neuroinflammation. *J Neurosci Res* (2018) 96(6):1002–20. doi: 10.1002/jnr.24150

29. Vallée A, Lecarpentier Y, Guillevin R, Vallée JN. Circadian rhythms, neuroinflammation and oxidative stress in the story of parkinson's disease. *Cells* (2020) 9(2):314. doi: 10.3390/cells9020314

30. Musiek ES, Xiong DD, Holtzman DM. Sleep , circadian rhythms , and the pathogenesis of Alzheimer disease. *Exp Mol Med* (2015) 47(3):e148–8. doi: 10.1038/emm.2014.121

31. Chen S, Fuller KK, Dunlap JC, Loros JJ. A pro- and anti-inflammatory axis modulates the macrophage circadian clock. *Front Immunol* (2020) 11(May):9–21. doi: 10.3389/fimmu.2020.00867

32. Shimohama S, Tanino H, Kawakami N, Okamura N, Kodama H, Yamaguchi T, et al. Activation of NADPH oxidase in alzheimer's disease brains. *Biochem Biophys Res Commun* (2000) 273(1):5–9. doi: 10.1006/bbrc.2000.2897

33. Gao HM, Zhou H, Hong JS. NADPH oxidases: Novel therapeutic targets for neurodegenerative diseases. *Trends Pharmacol Sci* (2012) 33(6):295–303. doi: 10.1016/j.tips.2012.03.008

34. Hernandes MS, Café-Mendes CC, Britto LRG. NADPH oxidase and the degeneration of dopaminergic neurons in parkinsonian mice. *Oxid Med Cell Longev* (2013) 2013. doi: 10.1155/2013/157857

35. Griffin P, Dimitry JM, Sheehan PW, Lananna BV, Guo C, Robinette ML, et al. Circadian clock protein rev-erbα regulates neuroinflammation. *Proc Natl Acad Sci U.S.A.* (2019) 116(11):5102–7. doi: 10.1073/pnas.1812405116

36. Musiek ES, Holtzman DM, Fitzgerald GA, Musiek ES, Lim MM, Yang G, et al. Circadian clock proteins regulate neuronal redox homeostasis and neurodegeneration. *J Clin Invest* (2013) 123(12):5389–400. doi: 10.1172/JCI70317

37. Balsalobre A, Damiola F, Schibler U. A serum shock induces circadian gene expression in mammalian tissue culture cells. *Cell* (1998) 93:929–37. doi: 10.1016/S0092-8674(00)81199-X

38. Xiang S, Mao L, Duplessis T, Yuan L, Dauchy R, Dauchy E, et al. Oscillation of clock and clock controlled genes induced by serum shock in human breast epithelial and breast cancer cells: Regulation by melatonin. *Breast Cancer (Auckl)* (2012) 6(1):137–50. doi: 10.4137/BCBCR.S9673

39. Clark GT, Yu Y, Urban CA, Fu G, Wang C, Zhang F, et al. Circadian control of heparan sulfate levels times phagocytosis of amyloid beta aggregates. *PLoS Genet* (2022) 18 (2):1–29. doi: 10.1371/journal.pgen.1009994

40. de Los Santos H, Collins EJ, Mann C, Sagan AW, Jankowski MS, Bennett KP, et al. ECHO: An application for detection and analysis of oscillators identifies metabolic regulation on genome-wide circadian output. *Bioinformatics* (2020) 36(3):773–81. doi: 10.1093/bioinformatics/btz617

41. Wang XL, Wolff SEC, Korpel N, Milanova I, Sandu C, Rensen PCN, et al. Deficiency of the circadian clock gene *Bmal1* reduces microglial immunometabolism. *Front Immunol* (2020) 11(December):1–13. doi: 10.3389/fimmu.2020.586399

42. Nakazato R, Hotta S, Yamada D, Kou M, Nakamura S, Takahata Y, et al. The intrinsic microglial clock system regulates interleukin-6 expression. *Glia* (2017) 65 (1):198–208. doi: 10.1002/glia.23087

43. Liu WW, Wei SZ, Huang GD, Liu LB, Gu C, Shen Y, et al. BMAL1 regulation of microglia-mediated neuroinflammation in MPTP-induced parkinson's disease mouse model. *FASEB J* (2020) 34(5):6570–81. doi: 10.1096/fj.201901565RR

44. Lively S, Schlichter LC. Microglia responses to pro-inflammatory stimuli (LPS, IFNγ+TNFα) and reprogramming by resolving cytokines (IL-4, IL-10). *Front Cell Neurosci* (2018) 12. doi: 10.3389/fncel.2018.00215

45. An J, Chen B, Kang X, Zhang R, Guo Y, Zhao J, et al. Neuroprotective effects of natural compounds on LPS-induced inflammatory responses in microglia. *Am J Transl Res* (2020) 12 (6):2353–78.

46. dos-Santos-Pereira M, Guimarães FS, Del-Bel E, Raisman-Vozari R, Michel PP. Cannabidiol prevents LPS-induced microglial inflammation by inhibiting ROS/NF-κB-dependent signaling and glucose consumption. *Glia* (2020) 68(3):561–73. doi: 10.1002/glia.23738

47. Guo D-K, Zhu Y, Sun H-Y, Xu X-Y, Zhang S, Hao Z-B, et al. Pharmacological activation of REV-ERBα represses LPS-induced microglial activation through the NF-κB pathway. *Acta Pharmacol Sin* (2019) 40(1):26–34. doi: 10.1038/s41401-018-0064-0

48. Ismail EN, Jantan I, Vidyadaran S, Jamal JA, Azmi N. Phyllanthus amarus prevents LPS-mediated BV2 microglial activation *via* MyD88 and NF-κB signaling pathways. *BMC Complement Med Ther* (2020) 20(1):202. doi: 10.1186/s12906-020-02961-0

49. Dai X-j, Li N, Yu L, Chen Z-y, Hua R, Qin X, et al. Activation of BV2 microglia by lipopolysaccharide triggers an inflammatory reaction in PC12 cell apoptosis through a toll-like receptor 4-dependent pathway. *Cell Stress Chaperones* (2015) 20(2):321–31. doi: 10.1007/s12192-014-0552-1

50. Tian Y, Zhu P, Liu S, Jin Z, Li D, Zhao H, et al. IL-4-polarized BV2 microglia cells promote angiogenesis by secreting exosomes. *Adv Clin Exp Med* (2019) 28(4):421–9. doi: 10.17219/acem/91826

51. Tang RH, Qi RQ, Liu HY. Interleukin-4 affects microglial autophagic flux. *Neural Regener Res* (2019) 14(9):1594–602. doi: 10.4103/1673-5374.255975

52. Latta CH, Sudduth TL, Weekman EM, Brothers HM, Abner EL, Popa GJ, et al. Determining the role of IL-4 induced neuroinflammation in microglial activity and amyloid-β using BV2 microglial cells and APP/PS1 transgenic mice. *J Neuroinflamm* (2015) 12(1):1–13. doi: 10.1186/s12974-015-0243-6

53. Simpson DSA, Oliver PL. Ros generation in microglia: Understanding oxidative stress and inflammation in neurodegenerative disease. *Antioxidants* (2020) 9(8):1–27. doi: 10.3390/antiox9080743

54. Gao HM, Liu B, Zhang W, Hong JS. Critical role of microglial NADPH oxidase-derived free radicals in the *in vitro* MPTP model of parkinson's disease. *FASEB J* (2003) 17(13):1–22. doi: 10.1096/fj.03-0109fje

55. Brandes RP, Weissmann N, Schröder K. Nox family NADPH oxidases: Molecular mechanisms of activation. *Free Radic Biol Med* (2014) 76:208–26. doi: 10.1016/j.freeradbiomed.2014.07.046

56. Sorce S, Stocker R, Seredenina T, Holmdahl R, Aguzzi A, Chio A, et al. NADPH oxidases as drug targets and biomarkers in neurodegenerative diseases: What is the evidence? *Free Radic Biol Med* (2017) 112(January):387–96. doi: 10.1016/j.freeradbiomed.2017.08.006

57. Hou L, Wang K, Zhang C, Sun F, Che Y, Zhao X, et al. Complement receptor 3 mediates NADPH oxidase activation and dopaminergic neurodegeneration through a src-erk-dependent pathway. *Redox Biol* (2018) 14(July 2017):250–60. doi: 10.1016/j.redox.2017.09.017

58. Panday A, Sahoo MK, Osorio D, Batra S. NADPH oxidases: An overview from structure to innate immunity-associated pathologies. *Cell Mol Immunol* (2015) 12(1):5–23. doi: 10.1038/cmi.2014.89

59. Nauseef WM. Assembly of the phagocyte NADPH oxidase. *Histochem Cell Biol* (2004) 122(4):277–91. doi: 10.1007/s00418-004-0679-8

60. Groemping Y, Rittinger K. Activation and assembly of the NADPH oxidase: A structural perspective. *Biochem J* (2005) 386(3):401–16. doi: 10.1042/BJ20041835

61. Qin L, Liu Y, Wang T, Wei SJ, Block ML, Wilson B, et al. NADPH oxidase mediates lipopolysaccharide-induced neurotoxicity and proinflammatory gene expression in activated microglia. *J Biol Chem* (2004) 279(2):1415–21. doi: 10.1074/jbc.M307657200

62. Mora-Pale M, Weïwer M, Yu J, Linhardt RJ, Dordick JS. Inhibition of human vascular NADPH oxidase by apocynin derived oligophenols. *Bioorg Med Chem* (2009) 17 (14):5146–52. doi: 10.1016/j.bmc.2009.05.061

63. Yu J, Weiwer M, Linhardt R, Dordick J. The role of the methoxyphenol apocynin, a vascular NADPH oxidase inhibitor, as a chemopreventative agent in the potential treatment of cardiovascular diseases. *Curr Vasc Pharmacol* (2008) 6(3):204–17. doi: 10.2174/157016108784911984

64. Hou L, Sun F, Huang R, Sun W, Zhang D, Wang Q. Inhibition of NADPH oxidase by apocynin prevents learning and memory deficits in a mouse parkinson's disease model. *Redox Biol* (2019) 22:101134. doi: 10.1016/j.redox.2019.101134

65. Hirano K, Chen WS, Chueng ALW, Dunne AA, Seredenina T, Filippova A, et al. Discovery of GSK2795039, a novel small molecule NADPH oxidase 2 inhibitor. *Antioxid Redox Signal* (2015) 23(5):358–74. doi: 10.1089/ars.2014.6202

66. Barua S, Kim JY, Yenari MA, Lee JE. The role of NOX inhibitors in neurodegenerative diseases. *IBRO Rep* (2019) 7(February):59–69. doi: 10.1016/j.ibror.2019.07.1721

67. Simons JM, Hart BA, Ip Vai Ching TR, Van Dijk H, Labadie RP. Metabolic activation of natural phenols into selective oxidative burst agonists by activated human neutrophils. *Free Radic Biol Med* (1990) 8(3):251–8. doi: 10.1016/0891-5849(90)90070-Y

68. Kosir R, Acimovic J, Golicnik M, Perse M, Majdic G, Fink M, et al. Determination of reference genes for circadian studies in different tissues and mouse strains. *BMC Mol Biol* (2010) 11. doi: 10.1186/1471-2199-11-60

69. Pintard C, Ben Khemis M, Liu D, Dang PMC, Hurtado-Nedelec M, El-Benna J. Apocynin prevents GM-CSF-induced-ERK1/2 activation and -neutrophil survival independently of its inhibitory effect on the phagocyte NADPH oxidase NOX2. *Biochem Pharmacol* (2020) 177(January):113950. doi: 10.1016/j.bcp.2020.113950

70. Dang DK, Shin EJ, Nam Y, Ryoo S, Jeong JH, Jang CG, et al. Apocynin prevents mitochondrial burdens, microglial activation, and pro-apoptosis induced by a toxic dose of methamphetamine in the striatum of mice *via* inhibition of p47phox activation by ERK. *J Neuroinflamm* (2016) 13(1):1–22. doi: 10.1186/s12974-016-0478-x

71. Kim DJ, Kim YS. Trimethyltin-induced microglial activation *via* NADPH oxidase and MAPKs pathway in BV-2 microglial cells. *Mediators Inflammation* (2015) 2015. doi: 10.1155/2015/729509

72. Yoo SH, Yamazaki S, Lowrey PL, Shimomura K, Ko CH, Buhr ED, et al. PERIOD2::LUCIFERASE real-time reporting of circadian dynamics reveals persistent circadian oscillations in mouse peripheral tissues. *Proc Natl Acad Sci U.S.A.* (2004) 101 (15):5339–46. doi: 10.1073/pnas.0308709101

73. Nakanishi H, Ni J, Nonaka S, Hayashi Y. Microglial circadian clock regulation of microglial structural complexity, dendritic spine density and inflammatory response. *Neurochem Int* (2021) 142:104905. doi: 10.1016/j.neuint.2020.104905

74. Lafaye G, Desterke C, Marulaz L, Benyamina A. Cannabidiol affects circadian clock core complex and its regulation in microglia cells. *Addict Biol* (2019) 24(5):921–34. doi: 10.1111/adb.12660

75. Ni J, Wu Z, Meng J, Saito T, Saido TC, Qing H, et al. An impaired intrinsic microglial clock system induces neuroinflammatory alterations in the early stage of amyloid precursor protein knock-in mouse brain. *J Neuroinflamm* (2019) 16(1):1–15. doi: 10.1186/s12974-019-1562-9

76. Coto-Montes A, Boga JA, Tomás-Zapico C, Rodríguez-Colunga MJ, Martínez-Fraga J, Tolivia-Cadrecha D, et al. Physiological oxidative stress model: Syrian hamster harderian gland - sex differences in antioxidant enzymes. *Free Radic Biol Med* (2001) 30 (7):785–92. doi: 10.1016/S0891-5849(01)00468-3

77. Anea CB, Zhang M, Chen F, Ali MI, Hart CMM, Stepp DW, et al. Circadian clock control of Nox4 and reactive oxygen species in the vasculature. *PLoS One* (2013) 8(10):1–10. doi: 10.1371/journal.pone.0078626

78. Wang Y, Pati P, Xu Y, Chen F, Stepp DW, Huo Y, et al. Endotoxin disrupts circadian rhythms in macrophages *via* reactive oxygen species. *PLoS One* (2016) 11(5):1–23. doi: 10.1371/journal.pone.0155075

79. Dohi K, Ohtaki H, Nakamachi T, Yofu S, Satoh K, Miyamoto K, et al. Gp91 phox (NOX2) in classically activated microglia exacerbates traumatic brain injury. *J Neuroinflammation* (2010) 7:41. doi: 10.1186/1742-2094-7-41

80. Kumar A, Barrett JP, Alvarez-Croda DM, Stoica BA, Faden AI, Loane DJ. NOX2 drives M1-like microglial/macrophage activation and neurodegeneration following experimental traumatic brain injury. *Brain Behav Immun* (2016) 58:291–309. doi: 10.1016/j.bbi.2016.07.158

81. Geng L, Fan LM, Liu F, Smith C, Li JM. Nox2 dependent redox-regulation of microglial response to amyloid-β stimulation and microgliosis in aging. *Sci Rep* (2020) 10 (1):1–11. doi: 10.1038/s41598-020-58422-8

82. Barrett JP, Henry RJ, Villapol S, Stoica BA, Kumar A, Burns MP, et al. NOX2 deficiency alters macrophage phenotype through an IL-10/STAT3 dependent mechanism: Implications for traumatic brain injury. *J Neuroinflamm* (2017) 14(1):1–17. doi: 10.1186/s12974-017-0843-4

83. Kröller-Schön S, Daiber A, Steven S, Oelze M, Frenis K, Kalinovic S, et al. Crucial role for Nox2 and sleep deprivation in aircraft noise-induced vascular and cerebral oxidative stress, inflammation, and gene regulation. *Eur Heart J* (2018) 39(38):3528–39. doi: 10.1093/eurheartj/ehy333

84. Alam ZI, Daniel SE, Lees AJ, Marsden DC, Jenner P, Halliwell B. A generalised increase in protein carbonyls in the brain in parkinson's but not incidental lewy body disease. *J Neurochem* (1997) 69(3):1326–9. doi: 10.1046/j.1471-4159.1997.69031326.x

85. Sengupta S, Lee Y, Tao JQ, Sehgal A, Chatterjee S. Circadian control of pulmonary endothelial signaling occurs *via* the NADPH oxidase 2-NLRP3 pathway. *bioRxiv* (2022). doi: 10.1101/2022.06.05.493624

86. Choi SH, Aid S, Kim HW, Jackson SH, Bosetti F. Inhibition of NADPH oxidase promotes alternative and anti-inflammatory microglial activation during neuroinflammation. *J Neurochem* (2012) 120(2):292–301. doi: 10.1111/j.1471-4159.2011.07572.x